Method for designing wave absorber: The wave absorber for a small sphere can be designed directly from the zero backscattering conditions for a coated conducting sphere such that the TE and the TM component of both E_θ and E_ϕ cancel each other out; i.e.

$$E_\theta^{TE} = -E_\theta^{TM} \quad (9)$$

$$E_\phi^{TE} = -E_\phi^{TM} \quad (10)$$

It can be seen from the above equations that three parameters need to be determined for a given radius of conducting sphere; the relative permittivity $\epsilon_r (= \epsilon_r' - j\epsilon_r'')$, the relative permeability $\mu_r (= \mu_r' - j\mu_r'')$, and the thickness of coating $d (= b - a)$. If two parameters including the thickness of the coating are fixed, the remaining parameter which satisfies eqns. 9 and 10 can be numerically searched for via the Newton-Raphson method. The initial guess for the numerical search can be obtained from the value obtained by plane absorber theory [7, 8].

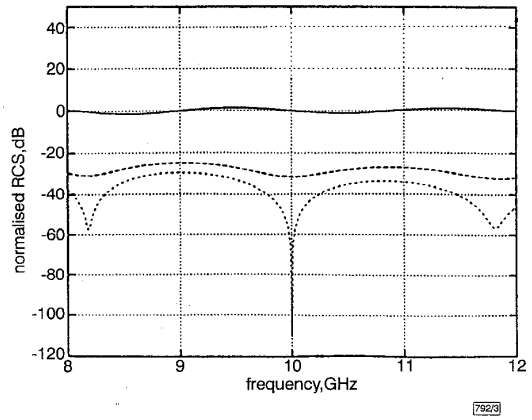

Fig. 3 *Normalised RCS for coated sphere in X-band*

——— conducting sphere
– – – – coated sphere from $a = \infty$
····· coated sphere from $a = 1\lambda_o$

Numerical results: Fig. 2 shows the change in μ_r' and μ_r'' for the zero backscattering condition when ϵ_r is fixed to $(2, -j0.5)$ and the thickness of coating is increased from $d = 0.05\lambda_o$ to $d = 0.33\lambda_o$. The line with $a = \infty$ shows the nonreflection condition of the plate-type absorber, and the other with $a = 1\lambda_o$ shows the perfect absorbing condition for a conducting sphere with radius $1\lambda_o$. It can be observed from Fig. 2 that two curves show a similar tendency when the coating is thin. Fig. 3 shows the normalised RCS for the coated sphere in the X-band (8–12GHz). The radius of the conducting sphere is 3cm ($a = 1\lambda_o$ at 10GHz) and the thickness of coating is 5.55 mm ($d = 0.185\lambda_o$ at 10GHz), respectively. The relative permeability from the nonreflection condition of the plate-type absorber and that obtained by this method are $\mu_r = (0.63115, -j0.52993)$ and $\mu_r = (0.64998, -j0.49441)$, respectively, when $\epsilon_r = (2., -j0.5)$ and $d = 0.185\lambda_o$ are given.

Conclusions: A method for designing a wave absorber for small spheres has been presented. When the radius of a conducting sphere is small in terms of the wavelength, absorbers designed by flat plate absorber theory will not have maximum absorption performance since curvature effects on the reflection coefficient and creeping wave diffraction are not included in the design of the wave absorber. The method suggested here can also be applied to a large conducting sphere, but the design parameters are not very different from those obtained by flat plate absorber theory. An absorber designed using this method will exhibit superior absorption performance to that obtained using flat plate absorber theory for a conducting sphere whose radius is $1\lambda_o$.

23 July 1998
Electronics Letters Online No: 19981329

Jaeruen Shim and Hyo-Tae Kim (*Department of Electrical Engineering, Pohang University of Science and Technology, Hyoja-dong, Pohang, Kyungbuk, 790-784, Korea*)

E-mail: jrshim@mom.postech.ac.kr, htkim@mom.postech.ac.kr

References

1 BHATTACHARYYA, A.K., and SENGUPTA, D.L.: 'Radar cross section analysis and control' (Artech House, 1991)
2 McNAMARA, D.A., PISTORIUS, C.W., and MALHERBE, J.A.G.: 'Introduction to the uniform geometrical theory of diffraction' (Artech House, 1990)
3 BOWMAN, J.J., and WESTON, V.H.: 'The effect of curvature on the reflection coefficient of layered absorbers', *IEEE Trans.*, 1966, **AP-14**, (6), pp. 760–767
4 HASHIMOTO, O., and MIZOKAMI, O.: 'A method for designing wave absorber for cylindrical objects', *IEEE Trans.*, 1991, **AP-39**, (6), pp. 854–857
5 KIM, H.T.: 'High-frequency analysis of EM scattering from a conducting sphere coated with a composite material', *IEEE Trans.*, 1993, **AP-41**, (12), pp. 1665–1674
6 HARRINGTON, R.F.: 'Time harmonic electromagnetic fields' (McGraw-Hill, 1961)
7 MUSAL, H.M., and HAHN, H.T.: 'Thin-layer electromagnetic absorber design', *IEEE Trans.*, 1989, **MAG-25**, (5), pp. 3851–3853
8 PESQUE, J.J., BOUCHE, D.P., and MITTRA, R.: 'Optimization of multilayer antireflection coatings using an optimal control method', *IEEE Trans.*, 1992, **MTT-40**, (9), pp. 1789–1796

Efficient determination of Q factor by structured nonorthogonal FDTD method

Yang Hao and C.J. Railton

A structured nonorthogonal finite-difference time-domain (FDTD) method incorporating existing perturbation techniques is used to determine the Q factor of an arbitrary three-dimensional cavity resonator. The new scheme combines the efficiency of the Cartesian mesh with the accuracy of the conformal grid. Good results are achieved with little computational effort.

It is well-known that the finite-difference time-domain method [1] is an efficient numerical algorithm in computational electromagnetics. However, in the original scheme, it is hard to deal with electromagnetic structures with curved boundaries. It has been proved that the staircase approximation of the physical boundary of a cavity resonator will often result in failure to detect all the resonant modes and inaccuracies in the prediction of the Q factors.

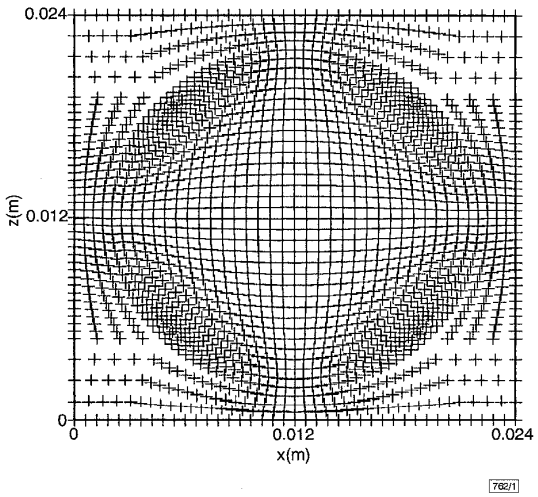

Fig. 1 *FDTD mesh for cylindrical resonant cavity*

For resonant structures which are axially symmetrical, cylindrical co-ordinates for a body of revolution (BOR) have been successfully used to determine the resonant modes and predict the Q factors [6]. Unfortunately, the scheme is limited to those regularly axially symmetrical structures, and, in fact, this curvilinear co-ordinate system may have singularities at isolated points such as the origin in a polar system.

In this Letter, we use this localised nonorthogonal FDTD scheme [4, 5] combined with the traditional perturbation technique to calculate the Q factor of a cavity resonator. All advantages of the FDTD method for the prediction of Q factors will be retained; moreover, as we use conformal grids at the curved boundary in the Cartesian co-ordinate system, the calculation of the tangential components of the electric and magnetic fields can be exactly achieved with little computational effort. This scheme can be readily extended to arbitrary resonant structures without being limited to a specified curvilinear co-ordinate system.

By the use of vector analysis, the electric and magnetic fields at the curved boundaries can be determined by their covariant and contravariant components [3]. The equations for the iteration of the discretised electric and magnetic fields are as follows:

$$E^x(i,j,k)^{n+1} = \frac{1-\frac{\sigma\delta t}{2\varepsilon}}{1+\frac{\sigma\delta t}{2\varepsilon}} \cdot E^x(i,j,k)^n + \frac{\delta t}{c\varepsilon}\cdot\sqrt{\frac{1}{g}}\cdot\frac{1}{1+\frac{\sigma\delta t}{2\varepsilon}}[H_y(i,j,k-1) - H_y(i,j,k) + H_z(i,j,k) - H_z(i,j-1,k)]^{n+\frac{1}{2}}$$

$$H^y(i,j,k)^{n+\frac{1}{2}} = H^y(i,j,k)^{n+\frac{1}{2}} + \frac{\delta t}{c\mu}\cdot\sqrt{\frac{1}{g}}\cdot[E_z(i+1,j,k) - E_z(i,j,k) - E_x(i,j,k+1) + E_x(i,j,k)]^{n-\frac{1}{2}}$$

$$E_x(i,j,k) = g_{xx}E^x(i,j,k) + \frac{g_{xz}}{4}[E^z(i+\tfrac{1}{2},j,k-\tfrac{1}{2}) + E^z(i-\tfrac{1}{2},j,k-\tfrac{1}{2}) + E^z(i+\tfrac{1}{2},j,k+\tfrac{1}{2}) + E^z(i-\tfrac{1}{2},j,k+\tfrac{1}{2})] + \frac{g_{xy}}{4}[E^y(i+\tfrac{1}{2},j-\tfrac{1}{2},k) + E^y(i-\tfrac{1}{2},j-\tfrac{1}{2},k) + E^y(i+\tfrac{1}{2},j+\tfrac{1}{2},k) + E^y(i-\tfrac{1}{2},j+\tfrac{1}{2},k)] \quad (1)$$

where σ is the conductivity of the metallic surface of the resonant cavity, μ is the permeability and ε is the permittivity of the material.

In [6], it has been demonstrated that the perturbation technique is very efficient and convenient for solving high Q and extra-high Q value resonant problems. In this Letter, it is assumed that the resonant cavity is filled with lossless material, and then only the conductor loss is considered. The Q factor determined by the perturbation method can be written as follows [6]:

$$Q_c = \frac{2}{\delta}\frac{\int_v \mu|\tilde{H}|^2 dv}{\oint_s \mu|\tilde{H}_t|^2 ds}$$

where δ is the skin depth of the conductor wall and H_t is the magnetic field tangential to the cavity wall. In the nonorthogonal co-ordinate system, the above equation can be denoted as eqn. 2:

$$Q_c = \frac{2}{\delta}\cdot\frac{A}{B}$$

$$A = \sum_{i,j,k}\mu(i,j,k)\cdot|\tilde{H}(i,j,k)|^2\cdot\sqrt{g(i,j,k)}$$

$$B = \sum_{i,j,k}\mu(i,j,k)\cdot\Big[|\tilde{H}_x(i,j,k)|^2\cdot\sqrt{g_{yy}\cdot g_{zz}-g_{yz}^2} + |\tilde{H}_y(i,j,k)|^2\cdot\sqrt{g_{xx}\cdot g_{zz}-g_{xz}^2} + |\tilde{H}_z(i,j,k)|^2\cdot\sqrt{g_{yy}\cdot g_{xx}-g_{xy}^2}\Big] \quad (2)$$

where $|\tilde{H}(i, j, k)|$ denotes the discrete Fourier transform of the magnetic fields at cell (i, j, k), and g_{mn} $(m, n = x, y, z)$ represents the metric tensor of the electric and magnetic fields; this is the important factor for determining the geometry of the curved structures and the time step, which should be carefully chosen for stability [3]. Note that x, y and z in eqn. 2 are generalised co-ordinates instead of the Cartesian co-ordinates.

To determine the Q factor, the following procedures are performed:

(1) excite the resonator with a short Gaussian pulse, and calculate the electromagnetic field distribution in the time domain at a certain position in the cavity

(2) perform an FFT on the time-domain signal and determine the resonant modes and resonant frequencies f_0 for each mode in the cavity

(3) run the FDTD program again but, after each iteration, update a DFT using eqn. 3 for the H field inside the cavity and on the surface of the cavity:

$$\mathrm{Re}\{\tilde{H}_{x,y,z}(i,j,k)\} = \mathrm{Re}\{\tilde{H}_{x,y,z}(i,j,k)\} + \cos(2\pi f_0\cdot niter\cdot\delta t)\cdot H_{x,y,z}(i,j,k)$$
$$\mathrm{Im}\{\tilde{H}_{x,y,z}(i,j,k)\} = \mathrm{Im}\{\tilde{H}_{x,y,z}(i,j,k)\} - \sin(2\pi f_0\cdot niter\cdot\delta t)\cdot H_{x,y,z}(i,j,k) \quad (3)$$

where $H_{x,y,z}(i, j, k)$ is the magnetic field in the time domain, *niter* is the iteration number and f_0 is the resonant frequency

(5) calculate the Q factor using eqn. 2 with the H field obtained from eqn. 3.

Table 1: Some resonant frequencies and Q factors in cylindrical cavity

Modes	From new FDTF scheme	Theoretical results	Q factors from this scheme	Theoretical Q factors [6]
	GHz	GHz		
TM_{010}	11.313	11.483	9654	9729
TE_{111}	12.58	13.314	10286	10868
TM_{011}	15.18	15.227	8000	8002
TM_{110}	17.38	18.300	12243	12281

The scheme is verified by using the example structure shown in Fig. 1. The cylindrical cavity has radius = 1cm and height = 1.5cm and is meshed by $40 \times 36 \times 40$ cells. The algorithm runs for 16384 time steps. The conductivity of the cavity is $\sigma = 5.8 \times 10^7$ Ω/m. Table 1 shows some resonant frequencies from this new scheme, and they are in a good agreement with the theoretical results. Fig. 2 shows the Q factors of the TE_{111} modes in the resonant cavity which are obtained by the nonorthognal FDTD method and the convergence to the final value as the number of FDTD time steps is increased.

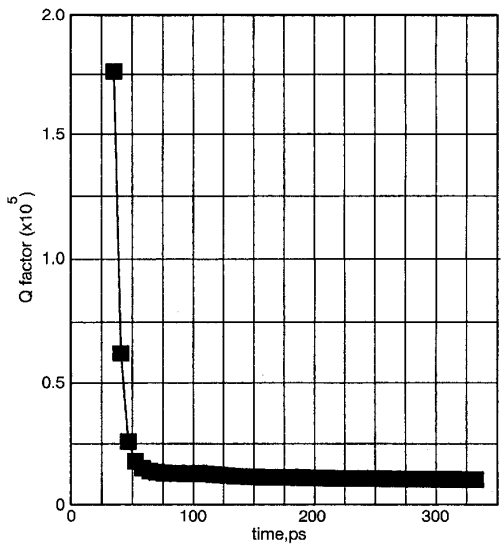

Fig. 2 *Q factors of TE_{111} mode and its convergence*
■ TE_{111} mode

In conclusion, a localised structured nonorthogonal FDTD method for predicting the resonant frequencies and Q factors in a cylindrical resonant cavity is presented. The resonant structure is meshed by structured grids and has no limitation to its geometry. It has the benefit of requiring reduced computer resources and can be readily extended to more complicated resonant structures.

Electronics Letters Online No: 19981314 *22 July 1998*

Yang Hao and C.J. Railton (*Centre for Communications Research, Faculty of Engineering, University of Bristol, Bristol, BS8 1UB, United Kingdom*)

References

1 YEE, K.S.: 'Numerical solution of initial boundary value problems involving Maxwell's equations in isotropic media', *IEEE Trans.*, 1966, **AP-14**, pp. 302–307
2 HOLLAND, R.: 'Finite difference solutions of Maxwell's equations in generalized nonorthogonal coordinates', *IEEE Trans.*, 1983, **NS-30**, (6), pp. 4589–4591
3 HARMS, P.H., LEE, J.F., and MITTRA, R.: 'A study of the nonorthogonal FDTD method versus the conventional FDTD technique for computing resonant frequencies of cylindrical cavities', *IEEE Trans.*, 1992, **MTT-40**, pp. 741–746
4 HAO, Y., and RAILTON, C.J.: 'Analysing electromagnetic structures with curved boundaries on cartesian FDTD meshes', *IEEE Trans.*, 1998, **MTT-46**, pp. 82–88
5 HAO, Y., and RAILTON, C.J.: 'Efficient and accurate FDTD algorithm for the treatment of curved material boundaries', *IEE Proc. H*, Oct. 1997, pp. 382–388
6 WANG, C., GAO, B.Q., and DENG, C.P.: 'Accurate study of Q-factor of resonator by a finite-difference time-domain method', *IEEE Trans.*, 1995, **MTT-43**, (7), pp. 1524–1529

Fast nonlinear diffusion approach for object segmentation

E. Izquierdo M. and M. Ghanbari

A low-complexity anisotropic diffusion technique for smoothing textures preserving object contours is presented. Additional features such as disparity or motion can be used to control the evolution of the intensity diffusion. Drastic simplifications in the iterative diffusion process are also introduced to reduce the algorithmic complexity.

Introduction: The process of image segmentation by anisotropic diffusion is usually carried out by solving a system of nonlinear partial differential equations of porous medium type, with the original image as the initial condition [1]. The evolution of the diffusion process obtained by solving such a system yields a three dimensional solution space. Regarding the segmentation task we are not concerned with the estimation of the whole surface obtained when the differential equation is solved continuously in time. A cross-section of the surface at a particular time t describes the diffusion result in which we are interested (see Fig. 1). For instance, in the case of linear isotropic diffusion modelled by the heat equation, for any evolution time the cross-section is given by the convolution of the initial datum with a Gaussian kernel with width proportional to $\sqrt{t}$. Analogously, selective smoothing by nonlinear diffusion can also be performed by weighted Gaussian filtering instead of solving a complex system of nonlinear differential equations. Moreover, to extract masks describing the shape of physical objects from stereoscopic images, the coefficients of the Gaussian kernels are calculated adaptively for each sampling position depending on the image gradient and the variations in the disparity field.

Adaptive smoothing: The filtering process is carried out taking into account information extracted from previously estimated disparity fields. These fields are obtained by using the low-complexity disparity estimator introduced in [2, 3]. In extracting object masks, we propose to distinguish three types of regions:

(*a*) regions with abrupt disparity variations and high intensity entropy; these regions indicate the presence of an object border
(*b*) regions with smooth disparity variations, but high intensity variations; these regions are probably part of one object
(*c*) regions with smooth intensity variations; in these regions, the results of disparity estimation are usually unreliable, but they probably constitute parts of one object or background.

Our selective smoothing procedure treats these three types of regions in a different way. We apply anisotropic (intensity-edge controlled) diffusion to regions of type *a*, while isotropic diffusion (regardless of intensity variations) is performed in type *b*. Regions of type *c* are homogenised in a much simpler way: for each connected uniform area, the average of intensity values over the whole area is assigned to all sampling positions. At the same time, we mark an intensity smoothness label field $IS(z)$, which is set to 1 at smooth area positions, and 0 elsewhere. All picture elements marked with 1 are then excluded from the iterative Gaussian smoothing.

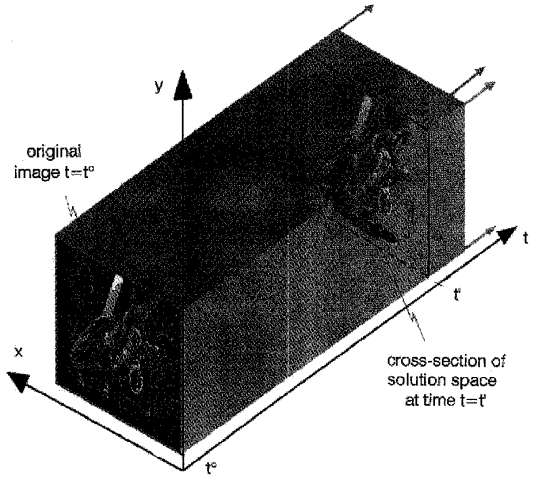

Fig. 1 *Continuous solution surface of diffusion equation with original image as initial value*

Cross-section of surface gives processed image as required

The degree of smoothness $DS(z)$ of the disparity field at any sampling position $z = (x, y)$ is obtained by measuring the variance of the disparity vectors inside a small observation window W centred at z:

$$DS(z) = \sigma^2_{z,W} = \sqrt{(\sigma^2_x)^2 + (\sigma^2_y)^2}$$

where (σ^2_x) and (σ^2_y) are the variances of the horizontal and vertical components of the disparity vectors inside the window W.

The Gaussian convolution kernel of size $N \times N$ is adapted at each sampling position z, unless the intensity smoothness label $IS(z) = 1$. Let $G = (c_{ij})$, $i, j = 1, ..., N$ be the Gaussian convolution kernel and denote $I(z_{ij})$ $i, j = 1, ..., N$ as the intensity values within the filter window around z and $\nabla I(z_{ij})$, $i, j = 1, ..., N$, the respective gradients. We then define the local gradient and intensity variations as $d_{ij} = |\nabla I(z) - \nabla I(z_{ij})|$ and $e_{ij} = |I(z) - I(z_{ij})|$, $i, j = 1, ..., N$. The weighted convolution kernel is estimated by multiplying each element c_{ij} of G by a non-negative weight $w_{ij} \in [0, 1]$, $i, j = 1, ..., N$, which is calculated by

$$w_{ij} = \left[f(d_{ij}) \cdot g(e_{ij})\right] \cdot \left[1 - h(DS(z))\right] + h(DS(z)) \quad (1)$$

$f(\cdot)$, $g(\cdot)$ and $h(\cdot)$ are continuous decreasing functions. Moreover $f(x) = 1$ if $x \le k_1$, $f(x) = 0$ if $x \ge 2k_1$, $g(x) = 1$ if $x \le k_2$, $g(x) = 0$ if $x \ge 2k_2$, $h(x) = 1$ if $x \le k_3$, $h(x) = 0$ if $x \ge k_4$. Note that the parameters k_1, k_2, k_3 and k_4 control the directions in which it is allowed to diffuse freely.

Applying eqn. 1, the weighted convolution kernel $\hat{G}$ is defined as: $\hat{G} = (\gamma_{ij})$, with

$$\gamma_{ij} = c_{ij} \cdot w_{ij} \Big/ \sum_{i,j=1}^{n} c_{ij} \cdot w_{ij} \quad \text{and} \quad i, j = 1, ..., N$$

In natural scenes, regions with smooth disparity variation and uniform regions typically constitute a large part of the image. For this reason, the application of anisotropic diffusion only in the remaining areas reduces the amount of necessary computations considerably. However, to speed up the convergence of the diffusion process even further, a suitable thresholding strategy is applied after each diffusion iteration, to regions of type *a* and *b*.

Results: The performance of the algorithm has been tested with several natural stereoscopic sequences. Here only selected results obtained by processing the sequence SAXO are reported. In all experiments the functions f and g in eqn. 1 are chosen to be linear. The scale parameter for the central excitatory region of the